Environmental Science Advances

ROYAL SOCIETY OF CHEMISTRY

PAPER

View Article Online
View Journal

Cite this: DOI: 10.1039/d6va00012f

Rising urban land surface thermal extremes in a rapidly evolving tropical Indian state

Dikshika Mahapatra and Debadatta Swain *

India, as a developing country is undergoing accelerated urbanization. However, this rapid and often unplanned urban growth has become a major concern as it significantly alters land surface characteristics. This leads to increased land surface temperatures (LSTs) which contribute to deteriorating air quality, energy overconsumption, and adverse health conditions, posing substantial challenges to sustainable urban climate management. The current study focuses on the identification and analysis of the evolution of thermal hotspots across 30 districts of Odisha, a rapidly developing tropical Indian state utilizing 20 years of datasets from the Moderate Resolution Imaging Spectroradiometer (MODIS) onboard Terra and Aqua, and Sentinel-2 satellite missions for the pre-monsoon season from 2017 to 2023. The analysis revealed that built-up areas exhibited significantly higher hotspot intensities than non-built-up regions. Districts with rapid population and industrial growth with extensive impervious surfaces and reduced vegetation showed a marked increase in thermal hotspots (at a maximum rate of 9% per year) emphasizing the role of impervious surfaces in modulating surface temperatures. In contrast, the percentage of hotspot coverage was higher over non-built-up areas for predominantly agrarian and semi-arid districts, likely due to the progressive decrease in vegetation cover from anthropogenic activity and consequent exposure of bare land. Furthermore, analysis indicated an intense prevalence of hotspots in rapidly urbanizing coastal districts with a minimum (maximum) increase of 2% (9%) area of hotspots in just seven years. These findings highlight the critical need for targeted mitigation strategies in urban areas facing intensified thermal stress.

Received 8th January 2026
Accepted 19th May 2026

DOI: 10.1039/d6va00012f

rsc.li/esadvances

Environmental significance

Rapid urbanization has driven extensive infrastructure growth and industrialization, leading to conversion of vegetated land to impervious surfaces. This transformation intensifies land surface temperature (LST) extremes, disrupting surface energy balance, exacerbating climate extremes, and increasing public health risks. This study evaluates evolving land surface thermal hotspots in the tropical state of Odisha, India, using high-resolution satellite based LST retrievals. The results show that built-up areas exhibit significantly higher hotspot intensities than non-built-up regions. Districts experiencing rapid population growth and industrial expansion demonstrate increases in thermal hotspots, reaching rates of up to 9% per year and for coastal districts ranging from 2% to 9% over seven years. These findings underscore the dominant role of impervious surfaces in regulating surface thermal regimes and also demonstrate the potential for *a priori* hotspot detection to support proactive and location-specific mitigation strategies.

1. Introduction

The increasing population and anthropogenic activities in rapidly developing countries have significantly impacted different natural land covers and associated surface properties.[1–3] Rapid infrastructure development and industrialization to accommodate the pressing needs of a fast-growing population are among the major factors affecting thermal comfort in urbanized cities.[4] Consequently, the land cover gets converted from vegetation to impervious surfaces like concrete, asphalt, and buildings, which retain more heat.[5–7] Hence, land use land cover (LULC) change is deemed as one of the major causes of increasing Land Surface Temperatures (LSTs) in urban areas.[8–10] This also leads to the Urban Heat Island (UHI) effect, which highlights the difference in temperature between an urban region and its surrounding rural regions.[11–13] The regions associated with very high LSTs contribute to the climate extremities, anomalous radiation budget, and significant environmental damage as well as health hazards.[14] The prevalence of these thermal hotspots directly translates into a degradation of urban environmental quality and poses significant risks to public health. Several studies have shown increasing LSTs to have a close correlation with air temperatures leading to elevated thermal exposure in urban regions[15,16] with the most immediate consequence of severe reduction in thermal comfort; and persistent high temperatures creating conditions of heat stress for urban dwellers.[17] Indirectly, higher

School of Earth, Ocean and Climate Sciences, Indian Institute of Technology Bhubaneswar, Argul, Jatni, Odisha, 752050, India. E-mail: dswain@iitbbs.ac.in

environmental temperatures could contribute to poorer air quality by accelerating the chemical reactions that form harmful ground-level ozone and increasing surface convection. This in turn could be a potent respiratory irritant, thereby creating a compounding public health challenge.[18,19] In addition, prolonged exposure to extreme heat, especially within these hotspots, elevates the risk of heat-related illnesses such as heat exhaustion, heat cramps, and life-threatening heatstroke.[20,21] The elevated thermal load can also exacerbate pre-existing chronic conditions, placing a dangerous strain on the cardiovascular and respiratory systems of vulnerable populations, including the elderly, children, and individuals with heart or lung disease.[18,22] Consequently, a detailed and precise identification of these high-temperature zones is essential for developing targeted mitigation of public health hazards and enhancing urban habitability.

Most of the earlier studies on LST variability and trends generally focused on the analysis of average LST changes over a region, which lacked the identification of localized effects.[23] Satellite-based thermal sensors are useful in identifying the "thermal hotspots" on the ground, which are regions showing consistently higher temperatures as compared to their surroundings.[24–27] The escalating challenge of thermal hotspot formation in dense tropical and Mediterranean built-up areas is increasingly tied to the nonlinear expansion of impervious surfaces. Recent research in megacities like Shanghai demonstrated that LST does not increase linearly with urbanization, and a critical threshold exists at approximately 40% impervious cover, beyond which heat accumulation intensifies disproportionately.[28] This phenomenon is exacerbated in semi-arid cities, where the conversion of vacant land to built-up infrastructure has created persistent thermal islands over the last decade.[29] In these environments, core urban zones frequently exhibited temperatures 4 °C to 5 °C higher than their rural counterparts, a trend particularly evident in Mediterranean climates, where residential hotspots accounted for 11% of the urban fabric.[30] The thermal hotspot occurrences are especially complicated by the spatiotemporal dynamics of coupled urban–thermal–ecological interactions, as seen in the western Himalayan foothills, where indices like the Normalized Difference Built-up Index (NDBI) and Bare Soil Index (BSI) showed strong positive correlations with LST, reaching coefficients as high as 0.78 and 0.82, respectively.[31] Moreover, the impact of these hotspots extended beyond environmental discomfort to economic consequences, as in Tehran, surface urban heat islands (SUHI) have been found to elevate urban temperatures by 5 °C to 12 °C, subsequently increasing annual building cooling energy demands by 15–20%.[32] Recent methodological shifts to local-scale microclimatic assessments emphasized the need for high-resolution, small-scale investigations to assess the true mitigation potential of nature-based solutions and policies.[33,34] Furthermore, the integration of multi-sensor data, including the use of Landsat-9 and Sentinel-2, allowed for a more granular identification of these thermal anomalies in recent times, ensuring that urban planning interventions could be directed toward the most vulnerable built-up sectors.[28,30]

A wide range of remote sensing sensors like Thematic Mapper (Landsat 4 & 5), Enhanced Thematic Mapper+ (Landsat 7), Thermal Infra-Red Sensor (Landsat 8 & 9), Moderate Resolution Imaging Spectroradiometer (MODIS onboard Terra and Aqua), Advanced Very High-Resolution Radiometer (AVHRR onboard MetOp), and Advanced Spaceborne Thermal Emission and Reflection (ASTER onboard Terra) are currently being utilized for obtaining LST. But, resolving rapid variations of LST over the highly heterogeneous land surfaces from coarse-resolution (30 m and above) satellite images still remains a challenge. This arises due to the satellite orbital constraints, creating a trade-off between their spatial and temporal resolutions.[35] To overcome this limitation, various studies have utilized downscaling techniques to generate LST data with high spatial and temporal resolutions.[36,37] Different approaches are used by researchers for LST downscaling, like the DisTrad (disaggregation of radiometric temperature) method, which is based on the linear relationship between LST and NDVI.[38] This is further modified as TsHARP (temperature sharpening), which considers NDVI as a regression kernel. Statistical regression-based methods like linear, multilinear, and non-linear approaches were widely used.[39,40] However, vegetation parameters alone cannot describe the LST variability in a complex terrain system. Along with NDVI, the Normalized Difference Built-up Index (NDBI) and Normalized Difference Bareness Index (NDBaI) are also some of the major factors related to LST in an urban region.[41–43] The current study is designed to identify the thermal hotspots by retrieving high-resolution LST over highly heterogeneous landscapes which are prone to the impacts of heat stress. An attempt is also made to demonstrate *a priori* detection of thermal hotspots which could contribute to expedite targeted mitigation strategies.

2. Study area, data, and methodology

2.1 Study area

The study focused on Odisha covering approximately 155 707 square kilometers, located on the eastern coast of India, between latitudes 17.78° N to 22.73° N and longitudes 81.37° E to 87.53° E (Fig. 1a). The state shares a 570 km coastal boundary with the Bay of Bengal to the east and is land-locked on the other three sides. The state also harbours diverse topographical features, ranging from coastal plains to mountains and plateaus. Odisha experiences a tropical climate characterized by hot summers, mild winters, and a monsoon season. This region has historically been a disaster and disease-prone area, with an abundance of vector-borne diseases like malaria, dengue, and Japanese encephalitis.[44] The state has emerged as a hub of major urban-industrial complexes in recent times, which has potentially increased the possible spread of such health hazards. The state of Odisha is broadly divided into four major geographical regions, namely Coastal Plains (CP), Central River Basins (CB), Northern Plateau (NP) and Eastern Hills (EH), as marked in Fig. 1b.[45] The districts are categorized as per these zones and numbered in the order of their population densities as per the 2011 Census (Table 1).[46] Fig. 1b and Table 1 also represent the elevation map of Odisha and the mean elevation of the 30 districts, as calculated from the NASA – Shuttle Radar Topography Mission Digital Elevation Model (SRTM DEM)

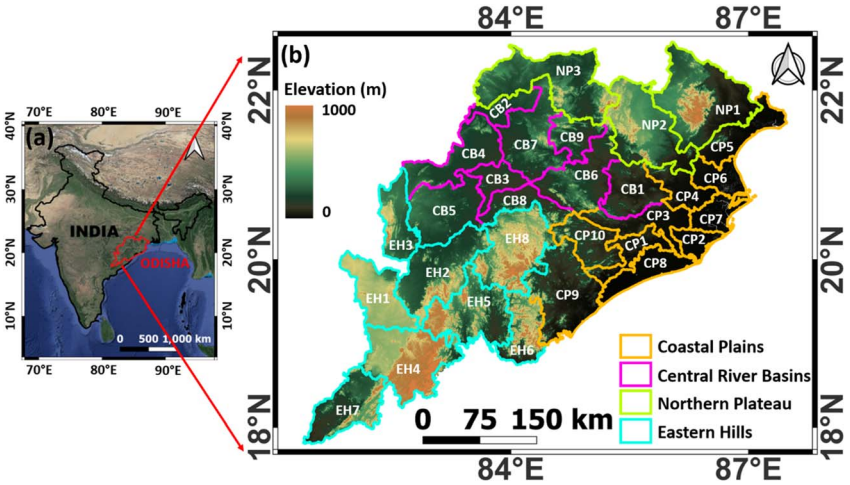

Fig. 1 (a) Location of Odisha and (b) district-level map (segregated into four geographical regions and numbered as per their population densities in 2011), along with the SRTM elevation data as the background.

Table 1 Demography of the 30 districts of Odisha in 2011 as per the Census,[46] and their mean elevation (metres above the mean sea level)[a]

Sl. no.	Name	Population density (per km^2)	Elevation (m)	Sl. no.	Name	Population density (per km^2)	Elevation (m)
CP1	Khordha	800.45	58.5	EH1	Nabarangpur	230.76	596.1
CP2	Jagatsinghpur	681.64	7.6	EH2	Kalahandi	199.09	376.7
CP3	Cuttack	667.46	65.1	EH3	Nuapada	158.45	382.3
CP4	Jajpur	630.28	53.3	EH4	Koraput	156.65	753.4
CP5	Baleswar	609.71	31.8	EH5	Rayagada	136.85	482.6
CP6	Bhadrak	601.33	9.9	EH6	Gajapati	133.59	520.1
CP7	Kendrapara	544.77	4.7	EH7	Malkangiri	105.88	336.1
CP8	Puri	488.28	6.8	EH8	Kandhamal	91.39	626.0
CP9	Ganjam	430.05	149.8	NP1	Mayurbhanj	241.86	308.2
CP10	Nayagarh	247.51	177.6	NP2	Keonjhar	216.99	376.5
CB1	Dhenkanal	275.79	113.1	NP3	Sundargarh	215.55	319.9
CB2	Jharsuguda	274.13	222.4				
CB3	Sonepur	261.09	141.6		Prefix	Geographical region	
CB4	Baragarh	253.77	226.3		CP	Coastal plains	
CB5	Balangir	250.79	240.6		CB	Central river basins	
CB6	Angul	199.81	214.8		EH	Eastern hills	
CB7	Sambalpur	157.17	260.0		NP	Northern plateau	
CB8	Boudh	142.40	208.9				
CB9	Deogarh	106.29	249.1				

[a] Districts in each zone are sorted based on their population density

available for the year 2000, respectively.[47] The district of Khordha was found to have the highest population density. This district which was also the most urbanized one included the capital city of Bhubaneswar. Kandhamal, which consists of dense forests and hills, had the lowest population density. Out of the 30 districts, Koraput is situated at the highest elevation while Kendrapara is at the lowest elevation above the mean sea level.

2.2 Data

Thermal hotspots play a crucial role in modulating the thermal comfort of a region. The peak thermal characteristics of the land surface are usually observed in the afternoon,[48,49] whereas high-resolution satellite imagery is available in the morning only over the Indian region (local pass time at around 10:30 h IST). Hence, there is a need for a high-resolution afternoon-time LST dataset to accurately identify urban thermal hotspots. For the analysis, Sentinel-2 surface reflectance data sets at 10:30 am IST available at 10 m spatial resolution and 5 days' temporal resolution were obtained from the Copernicus Browser (https://browser.dataspace.copernicus.eu/) for the pre-monsoon period spanning the years 2017 to 2023. Additionally, Sentinel-2 LULC data were obtained from ESRI Living Atlas repository (https://livingatlas.arcgis.com/en/home/) for the analysis period. Surface reflectance and LST data products from MODIS-Terra (MOD09A1.061 for reflectance) at 10:30 IST and

MODIS-Aqua (MYD09A1.061 for reflectance and MYD11A2.061 for LST) at 13:30 IST (afternoon) at 1 km spatial resolution were also obtained from NASA LP DAAC (https://www.earthdata.nasa.gov/data) for the pre-monsoon period of 2004 to 2023. This study developed a multi-sensor approach, combining Sentinel-2 (high resolution, available only in the morning) and MODIS-Terra/Aqua (moderate resolution, available during both morning and afternoon) satellite data to detect LST hotspots. MODIS LSTs for the pre-monsoon period from 2004 to 2023 were utilized to establish a long-term climatological baseline for LST estimation, while MODIS and Sentinel-2 data sets for the period 2017 to 2023 were utilized for the detailed analysis. A selective validation of Sentinel-2 derived LST was attempted over one of the districts during the pre-monsoon period in 2024 based on ground truth data availability. Yearly high-resolution population metrics for the 2017–2023 period were obtained from the WorldPop global population counts in 100 m × 100 m grids (https://hub.worldpop.org/geodata/listing?id=135) to investigate the risks owing to population density.

2.3 Methodology

The first step of the analysis involved computation of remote sensing indices from the available surface reflectances from MODIS and Sentinel-2. The normalized difference method was used to compute NDVI,[50] NDBI,[51] NDBaI[52] and NDMI[53] from appropriate spectral bands of the Sentinel-2 and MODIS, separately. These indices were then used in a two-stage regression formulation to obtain 10 m resolution LSTs at 13:30 h. First, a simple linear regression fit was established between MODIS morning and afternoon indices, using eqn (1).

$$y = mx + c \quad (1)$$

where x and y denote the morning and afternoon indices, while m and c represent the slope and intercepts, respectively. The resulting transfer functions were applied to morning Sentinel-2 indices, namely, NDVI, NDBI, NDBaI and NDMI to estimate afternoon indices at 10 m resolution. This was followed by the development of a multiple linear regression model relating MODIS-Aqua LSTs and indices, both available in the afternoon, using eqn (2).

$$\mathrm{LST} = m_1\mathrm{NDVI} + m_2\mathrm{NDBI} + m_3\mathrm{NDBaI} + m_4\mathrm{NDMI} + c \quad (2)$$

where m_1, m_2, m_3, m_4 and c are estimated model coefficients. This relation was thereafter applied to the 10 m Sentinel-2 afternoon indices to obtain downscaled LSTs at 10 m for 30 districts of Odisha. A methodological validation of Sentinel-2 derived LSTs was also carried out against Aqua-MODIS LST observations. This particular MODIS product is known to be a widely accepted benchmark in satellite-based thermal studies.[54–56] To enable direct comparison, 10 m Sentinel-2 LST pixels were spatially averaged to match the 1 km MODIS grid. Using an area-proportional stratified random sampling approach, widely used in geospatial comparisons,[57–59] 3234 MODIS pixels were selected across the 30 districts and statistically compared with the corresponding 1 km-averaged Sentinel-2 pixels of the same number. Furthermore, the downscaled LST was validated against *in situ* observations for the Khordha (CP1) district of Odisha during 2nd March and 11th May 2024.

The next step involved identification of thermal hotspots in all 30 districts. For this, a LST threshold value from the afternoon MODIS LST 20 years climatology was computed for each pixel over the study region. The LST was defined as the 90th

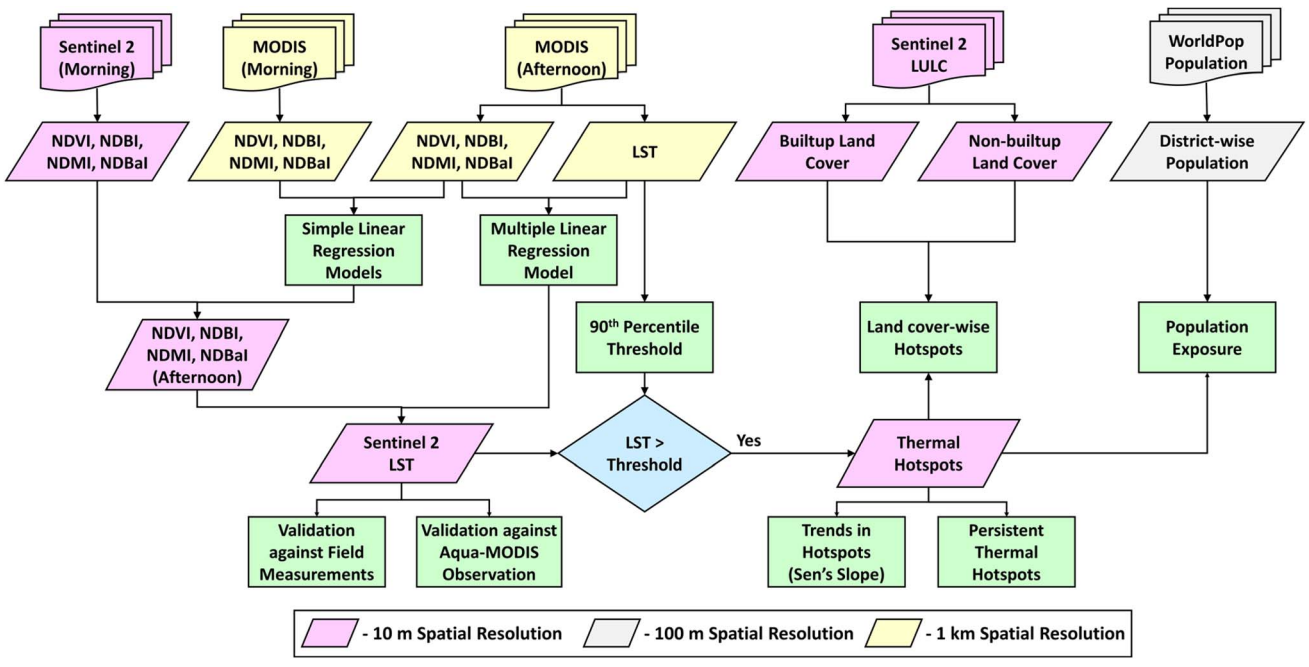

Fig. 2 Flowchart of the methodology.

percentile of the historical LST distribution.[60] This percentile-based approach ensures that a hotspot is classified as an area experiencing significantly higher temperatures relative to its own long-term thermal variability. The high-resolution LST derived from Sentinel-2 for the study period (2017–2023) was then compared against this baseline, and any pixel with an LST value exceeding the threshold was designated as a thermal hotspot. Additionally, Sentinel-2 LULC datasets were analysed to assess the influence of land cover change on hotspot occurrences during the study period. The LULC classes were first categorised into built-up and non-built-up. The built-up class encompassed impervious surfaces like urban infrastructure and industrial areas, while the non-built-up class consisted of all other land covers including vegetation, barren land, and agricultural fields. The total area and percentage area of hotspots over the two classes were then estimated for all the districts during the period 2017 to 2023. Evolution of thermal hotspots over time and the corresponding areas were quantified through trend analysis utilizing Sen's slope method. All statistical parameters presented in the current work were also examined for significance at a confidence level of 95%. Persistent thermal hotspots (PTHs) in all the districts were calculated by selecting the pixels that showed higher temperatures above the threshold value (90th percentile) for more than half the study period. Finally, population exposure was estimated as the number of persons exposed to thermal hotspots within a 100 m × 100 m grid, calculated using eqn (3). Since Sentinel-2 LST was derived at 10 m resolution, the maximum number of possible hotspot pixels in a 100 m × 100 m population grid was 100. Hence, the total population in a 100 m × 100 m grid was multiplied with the fraction of hotspots in that grid to calculate the total number of persons exposed to hotspots, assuming that the population distribution in that grid is homogeneous.[61] Percentage population exposure was calculated as the percentage of population of a district exposed to hotspots compared to its total population. Fig. 2 summarizes the overall methodology of the current study.

$$\text{Pop. Exp.} = \frac{(\text{No. of hotspot pixels})}{(\text{No. of total pixels})} \times \text{population} \quad (3)$$

3. Results and discussion

3.1 Thermal hotspots from downscaled LST

The downscaling approach combining Sentinel-2 and MODIS datasets was carried out to generate afternoon time LST at 10 m resolution over the study area. The descriptive statistics of LST (LST_{Mean} and LST_{SD}) were first analyzed to assess its spatio-temporal variations across the four zones of the study area, as presented in Fig. 3. In the CP districts, characterized by low altitude and high population density, a predominant warming trend was observed, with districts such as Ganjam (CP9), Baleswar (CP5), and the highly urbanized Khordha (CP1) showing positive LST trends. However, exceptions included Cuttack (CP3) and Bhadrak (CP6), which exhibited cooling LST trends. Cuttack has a unique geographical setting, a deltaic region bounded by two major rivers, Mahanadi and Kathajodi, on either side. This proximity to large streams of flowing waters could possibly result in the cooling trends, with water behaving as a localized thermal buffer owing to its high specific heat capacity.[62] Similarly, the cooling trends in Bhadrak could largely be driven by the expansive agricultural land which would enhance evaporative cooling through transpiration and close proximity to the Bay of Bengal sharing its boundary with the ocean.[63]

Moving to the CB districts, the trends were highly heterogeneous (Fig. 3). While Angul (CB6) exhibited a significant warming trend, likely due to industrial activity, Jharsuguda (CB2) displayed a sharp decline in mean LST, suggesting localized cooling factors or changes in land cover. The NP districts were defined by a striking contrast, where Mayurbhanj (NP1) exhibited the highest warming rate across the entire state, drastically diverging from its zonal counterparts, Keonjhar (NP2) and Sundargarh (NP3), which showed slight cooling. Conversely, the EH districts, situated at higher altitudes, displayed a consistent cooling trajectory across almost all districts, with Malkangiri (EH8) and Nuapada (EH3) recording the most substantial negative slopes, indicating that the high-altitude distinct geography may be experiencing a temperature stabilization or reduction compared to the warming signals observed in the lower-elevation, densely populated coastal and industrial districts. The standard deviation (grey bars) fluctuated annually throughout the districts, indicating inter-annual variability in temperature extremes. These often peaked in years like 2019 or 2022, depending on the specific zone. LST_{SD} was lower in CP districts as compared to the other zones. The distinct spatial pattern of such LST variations was likely driven by the moderating maritime influence of the Bay of Bengal, which provided a cooling and stabilizing effect to coastal districts.[64] Inland regions, lacking this effect and potentially influenced by local topography and land cover, experienced a stronger continental climate with more extreme heat.[65] Furthermore, the influence of urban morphology, such as increased shading in high-density and high-rise residential clusters, could contribute to lower surface temperatures compared to the expansive industrial surfaces.[66] These findings underscored the fact that while urbanization typically drives warming, local environmental and morphological factors can effectively modulate its intensity and extent.

To validate the downscaled LST, a methodological comparison between the derived Sentinel-2 LST and the Aqua-MODIS LST was first conducted (Fig. 4a). This showed a strong positive Pearson's correlation coefficient ($r = 0.83$), and a low root mean square error (RMSE) of 2.73 °C, confirming that the spatial patterns captured by Sentinel-2 LST were reasonably consistent with the MODIS benchmark considering the nature of the study. An earlier intercomparison by Andriambololonaharisoamalala *et al.* (2025)[67] also yielded a similar correlation ($r = 0.85$) and RMSE of 2.7 °C for a similar cross-platform LST downscaling framework. The small positive bias of 2.25 °C was likely due to the fact that Sentinel-2, even when aggregated, preserves thermal signatures from high thermal intensity surfaces (such as industrial roofs or bare rock) that may be more

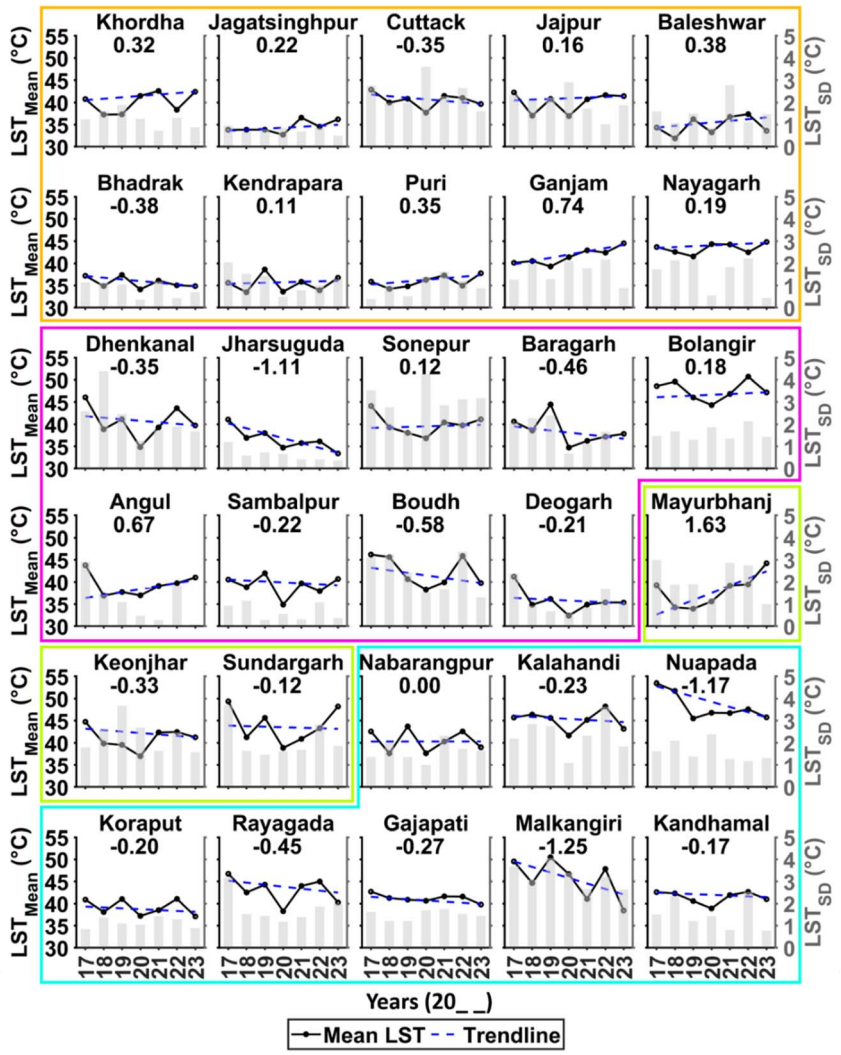

Fig. 3 Mean and standard deviation (SD) of LST, along with the trendline and Sen's slope statistics for the 30 districts of Odisha during the pre-monsoon season of 2017 to 2023.

heavily smoothed by the coarser resolution MODIS sensor. The overall clustering of data points demonstrated that the downscaling methodology effectively preserved the broad spatial thermal patterns and baseline radiometric characteristics of the original MODIS data and translated it into the derived high-resolution LST. Field validation of the derived high-resolution LST was carried out by inter-comparison with *in situ* observations for the Khordha district during the pre-monsoon season of 2024 (Fig. 4b and c). Three major land cover types were considered for validation, namely, barren land, vegetation, and built-up areas, involving 68 satellite and *in situ* collocated points. A moderate correlation of 0.54 was observed between the two datasets.[68] Additionally, the downscaled LSTs were found to be underestimated, as indicated by a bias of −4.9 °C, and RMSE of 5.3 °C. The observed discrepancy in error margins, *i.e.*, a lower error during the satellite-to-satellite methodological validation compared to the satellite-to-ground field validation, could be primarily attributed to spatial scale mismatch and land surface heterogeneity. The methodological validation compared two satellite-derived radiometric products that inherently averaged thermal signals over varying pixel areas, leading to stronger statistical agreement. Conversely, field observations represented highly localized point measurements that captured singular LSTs, which a satellite pixel inherently smoothed out.

The downscaled LST was then used to identify thermal hotspots by comparing them with the climatology. The hotspots over the Khordha district during the study period are presented in Fig. 5. The yellow boxes in Fig. 5 indicate the urban centers where thermal hotspots were the most prominent. In 2017, the hotspots were mainly distributed in the southern region of the district, while a significant decrease in hotspot area was observed during 2018 and 2019. In 2020, the hotspots started to increase again, mainly across the central and southern regions of the study area. However, the highest spread of thermal hotspots was observed in 2021, followed by 2023, exhibiting significant inter-annual variability.

Overall, the thermal hotspots over the Khordha region had an increasing trend in the past seven years. Since the overall temperatures are currently on the rise, it is only normal that

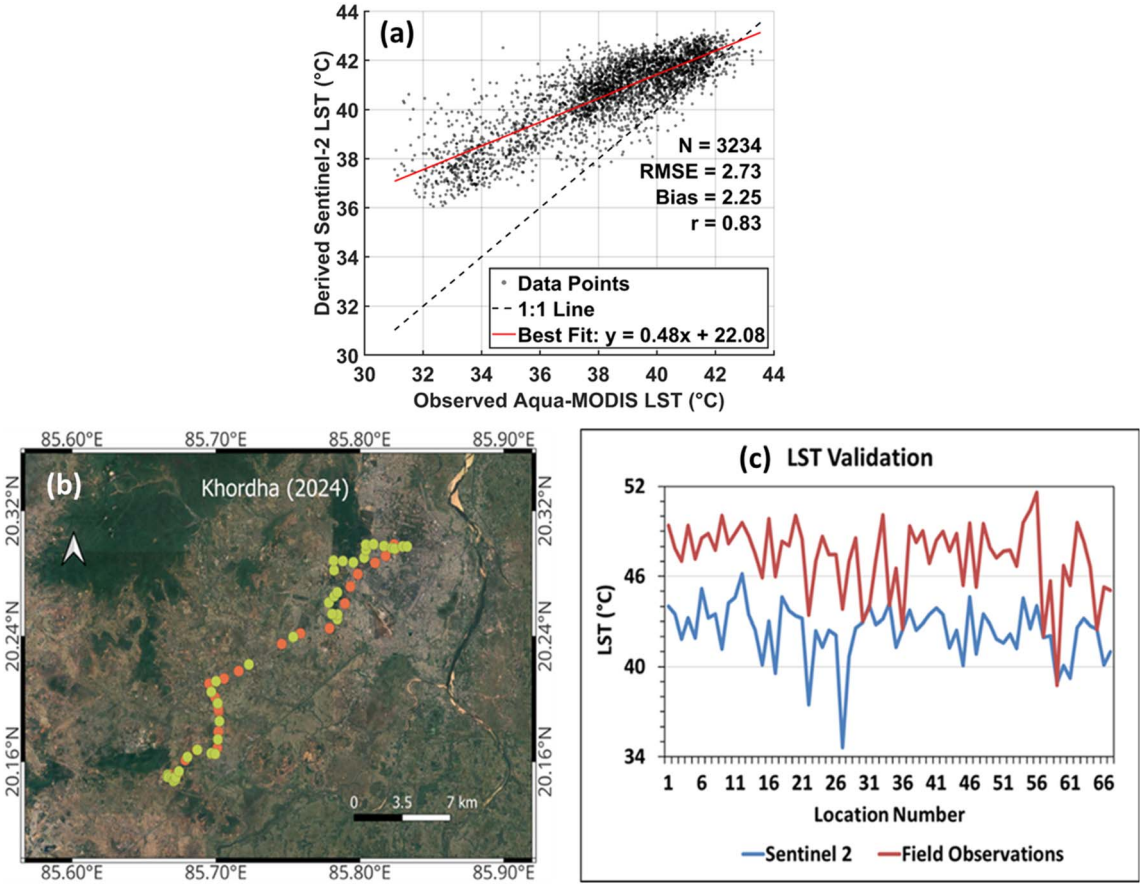

Fig. 4 (a) Methodological comparison between derived Sentinel-2 LST and observed Aqua-MODIS LST, with statistical and error metrics given on the plot. (b) Locations of *in situ* observation points in the Khordha district during 2nd March (orange dots) and 11th May (yellow dots) of the 2024 pre-monsoon season. (c) Inter-comparison of the derived Sentinel-2 LST against concurrent field measurements.

most regions are experiencing an increase in LST, sometimes even above the 90th percentile threshold. Consequently, thermal hotspots have been identified over several vegetated regions and fallow lands in the study area over the years. An example of such a region is the southwestern part of the Khordha district, where LST over a reserved forest was observed to be exceeding the 90th percentile threshold of its climatology. The detailed characterization of Khordha in this section was primarily due to its well-documented status as the most urbanized region in Odisha,[69] serving as a primary indicator for urban thermal stress. However, this phenomenon was not isolated to this single district. Similar extensive thermal hotspot occurrences were observed across various other districts throughout the state, driven by a diverse array of localized mechanisms including industrial expansion, open-cast mining, and severe forest degradation. Crucially, much like the patterns observed in Khordha, these widespread hotspots exhibited significant inter-annual variability across the study period, as detailed in the subsequent section.

3.2 Impact of land use land cover on thermal hotspot formation

Sentinel-2 LULC was used to assess the influence of land cover on the distribution of hotspots over the study area. The hotspots were broadly segregated into two categories, over built-up and non-non-built-up land covers. The percentage of hotspots over each of these two land covers is presented as grouped bar plots in Fig. 6. The *y*-axis represents the percentage of hotspot areas, while the *x*-axis corresponds to the districts numbered similar to Table 1. Built-up areas (red bars) comprise a significantly higher proportion of hotspots compared to non-built-up areas (blue bars), indicating the impact of urbanization on increasing thermal hotspots in recent years. It was observed that Khordha, Cuttack, Sambalpur, Sundargarh, Angul, and Jharsuguda, all highly urbanized and industrial districts, exhibited the highest percentage of hotspot areas over built-up land covers. The high thermal capacity of these built-up land covers makes these regions more prone to higher daytime temperatures and higher occurrences of thermal hotspots, as similarly observed in previous studies.[70,71] In contrast, hotspot areas in non-built-up land cover were notably higher in western and interior regions of Odisha in CB and EH zones, such as Bargarh, Balangir, Kalahandi and Nuapada. These districts, although previously agrarian, have recently experienced a prevalence of barren lands, fallow agricultural land, and areas impacted by deforestation. Such a change in the natural land covers diminishes the natural cooling effect and leads to elevated LSTs, which may have led to the formation of thermal hotspots over the non-

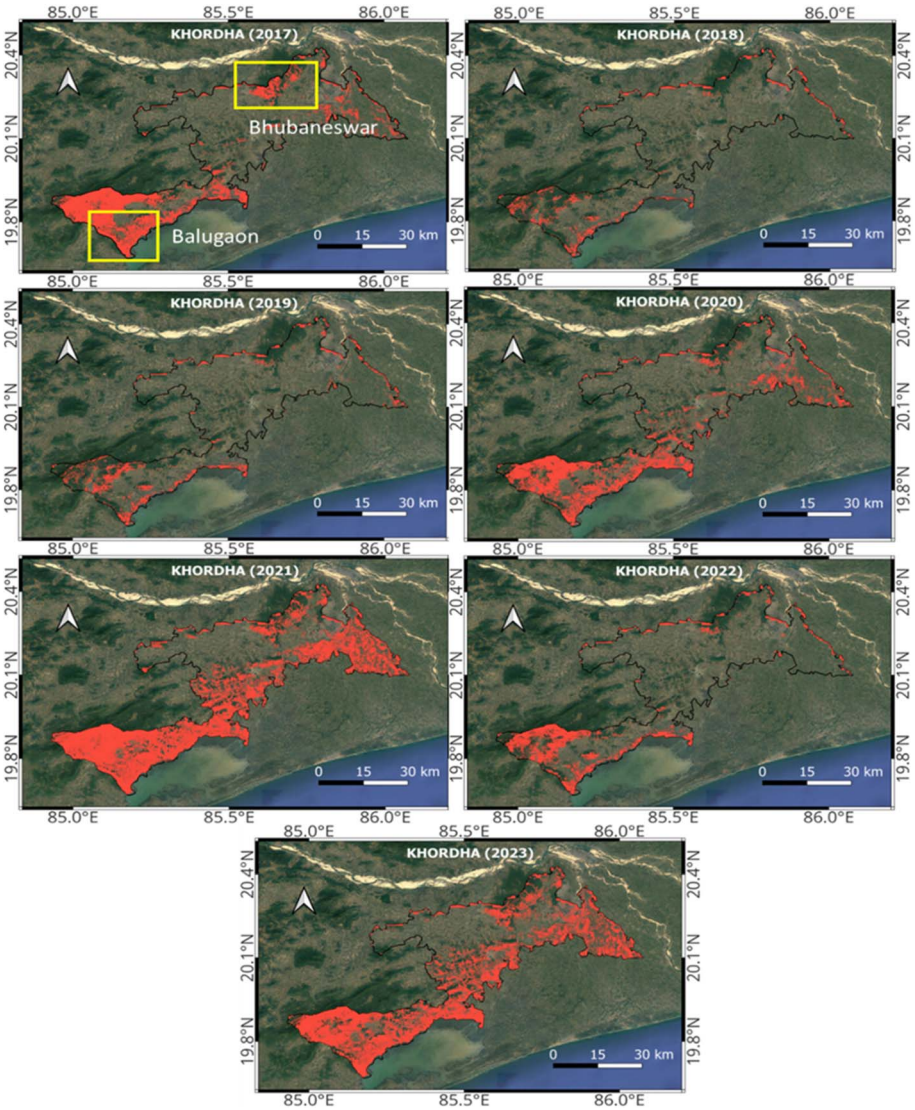

Fig. 5 Distribution of thermal hotspots during the pre-monsoon season of 2017 to 2023 over the Khordha district, Odisha.

built-up regions.[72] However, the Sundargarh district is unique in this sense, showing high hotspot areas in both built-up and non-built-up regions. This indicated a mix of urban and natural surface heating effects in the district. Overall, the results highlighted a clear pattern where urban centers in the NP and CP districts experienced a higher proportion of hotspots in built-up areas, while western and interior districts exhibited more heat concentration in non-built-up land covers.

Changes in the percentage cover of hotspots over built-up and non-built-up regions were estimated using a trend analysis. The rates of change of hotspot area (% per year) over built-up and non-built-up land covers across Odisha are shown in Fig. 7. From the figure, it is evident that certain coastal districts, such as Ganjam, Kendrapara, and Khordha, along with Balangir and Mayurbhanj, exhibited a significant increasing trend in hotspot areas over the built-up regions. Among these, the Ganjam district showed the highest rate of change in hotspots over both built-up and non-built-up land covers. Such trends are indicative of rapid urbanization and infrastructure expansion in these districts, leading to intensified land surface heating.[73] Similarly, districts like Gajapati, Nabarangpur, and Sonepur in the eastern hill regions also showed a significant rise in hotspot areas in both built-up and non-built-up regions. Conversely, several districts in the coastal and northern Odisha, including Cuttack, Balangir, Sundargarh, and Sambalpur, exhibited a decreasing trend in hotspot areas over built-up land, potentially reflecting increased vegetation or climate-related variations reducing heat accumulation. Interestingly, districts in the EH zone showed a decreasing percentage of hotspots over both built-up and non-built-up land covers. These districts are all situated at higher elevations (more than 200 m above the mean sea level), have low population densities, and are among the major vegetated regions of the state. Some districts, such as Jagatsinghpur and Dhenkanal, showed relatively low trends, showing minimal changes in hotspot areas over time.

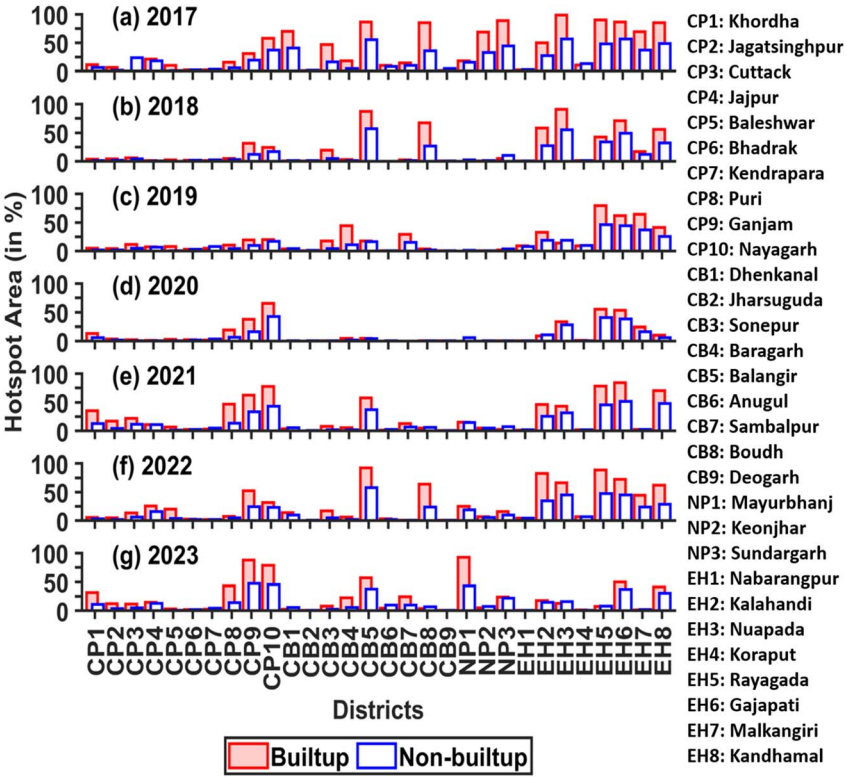

Fig. 6 Percentage of hotspot areas in built-up and non-built-up land cover across the 30 districts of Odisha. Panels a–g represent the years from 2017 to 2023, respectively.

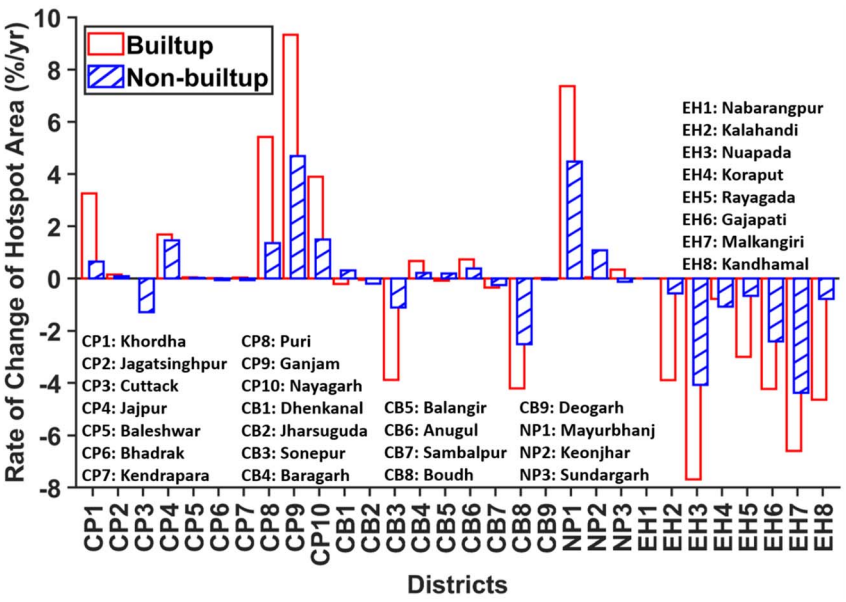

Fig. 7 Percentage change per year in hotspot area over built-up and non-built-up land covers across the 30 districts of Odisha.

3.3 Persistent thermal hotspot occurrences over Odisha

The spatial distribution of PTHs across Odisha revealed stark regional contrasts intimately tied to the state's four primary geographic typologies, driven by distinct land surface mechanisms. Table 2 presents a district-wise account of the total area and percentage of that area covered by PTHs for the 30 districts of Odisha. Fig. 8 depicts the spatial distribution of these PTH occurrences for the CP, CB, NP, and EH districts, respectively. In the CP districts, the region generally experienced low-to-moderate thermal vulnerability due to their coastal climate and

Table 2 Areal coverage of PTHs over the 30 districts of Odisha[a]

Sl. no.	Name	Area (km^2)	% area of the PTH	Sl. no.	Name	Area (km^2)	% area of the PTH
CP1	Khordha	2733.19	8.17	EH1	Nabarangpur	5260.06	3.66
CP2	Jagatsinghpur	1705.57	5.37	EH2	Kalahandi	7927.29	60.87
CP3	Cuttack	3897.49	16.93	EH3	Nuapada	3889.42	66.14
CP4	Jajpur	2880.89	18.62	EH4	Koraput	8624.38	4.07
CP5	Baleswar	3834.45	3.42	EH5	Rayagada	7397.67	92.09
CP6	Bhadrak	2510.02	4.22	EH6	Gajapati	4052.38	86.16
CP7	Kendrapara	2468.57	7.16	EH7	Malkangiri	5762.22	36.36
CP8	Puri	3596.38	20.91	EH8	Kandhamal	8057.16	62.56
CP9	Ganjam	8533.47	40.70	NP1	Mayurbhanj	10 444.80	27.93
CP10	Nayagarh	3892.92	76.05	NP2	Keonjhar	8307.68	5.61
CB1	Dhenkanal	4520.54	6.42	NP3	Sundargarh	9716.67	18.57
CB2	Jharsuguda	2105.96	2.64				
CB3	Sonepur	2376.07	9.68		Prefix	Geographical region	
CB4	Baragarh	5761.67	8.57		CP	Coastal plains	
CB5	Balangir	6642.63	75.02		CB	Central river basins	
CB6	Angul	6379.63	3.01		EH	Eastern hills	
CB7	Sambalpur	6720.26	14.24		NP	Northern plateau	
CB8	Boudh	3069.57	15.97				
CB9	Deogarh	2796.53	1.57				

[a] Districts in each zone are sorted based on their population density.

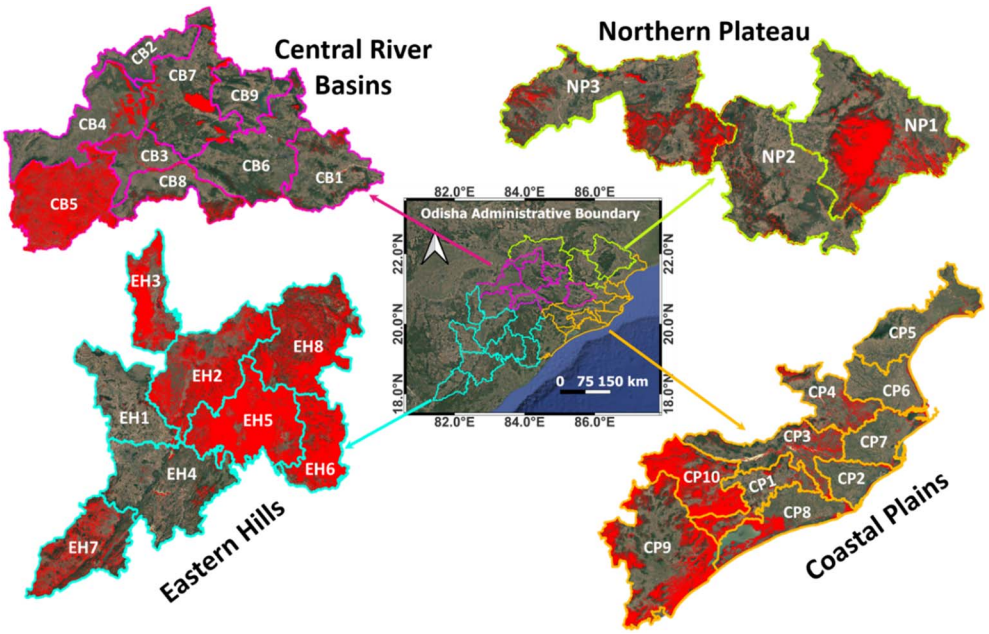

Fig. 8 PTH occurrences (in red) over the districts of Odisha.

moist deltaic soils. Northern districts like Baleswar (3.42%) and Bhadrak (4.22%) were observed to have minimal PTH coverage. However, severe exceptions emerged in Nayagarh (76.05%) and Ganjam (40.70%). In these areas, extreme heat heavily aligned with topographical heat trapping, exposed sandy shorelines, and the receding margins of shallow water bodies like Chilika Lake. Furthermore, dynamic urban land covers in rapidly urbanizing coastal cities experienced intense episodes of heat. However, the frequent alteration of land covers in these expanding urban centers often disrupted the temporal continuity needed to classify them as static, long-term PTHs. Moving inland to the CB districts, the thermal landscape transitioned into a more fragmented but intensely concentrated pattern. While the region contained highly stable thermal environments in districts like Deogarh (1.57%) and Angul (3.01%), Balangir (75.02%) stood out as a massive and contiguous thermal anomaly. Heat clusters in this typology were heavily sustained by established open mines and heavily modified industrial corridors that absorbed maximum solar radiation. Additionally, major river networks like the Mahanadi

and Brahmani actively contributed to localized thermal stress, as seasonally decreasing water levels exposed expansive, rapidly heating dry river beds. In the NP districts, a comparatively more variable susceptibility to persistent heating was observed. Extensive open mines and localized industrial clearings contributed to focused, severe heat clusters across this elevated terrain in the region. Finally, the EH districts demonstrated the most extensive and contiguous thermal vulnerability in the entire state. A record-high thermal stress engulfed Rayagada (92.09%) and Gajapati (86.16%), alongside a severe continuous belt covering Nuapada (66.14%), Kandhamal (62.56%), and Kalahandi (60.87%). This widespread, persistent heat could be primarily driven by the degradation of natural forests, extensive shifting cultivation, and the rapid pre-monsoon heating of barren rocky terrains. Only a few districts like Nabarangpur (3.66%) and Koraput (4.07%) maintained exceptionally low coverages, which could be attributed to surviving intact canopies and localized moisture retention.

Despite belonging to varying geographic typologies, the districts recording the most extreme thermal vulnerability, namely Kalahandi, Nuapada, Rayagada, Gajapati and Kandhamal in the EH region, Balangir in the CB region, and Nayagarh in the CP region, shared a critical underlying mechanism. Their exceptionally high PTH occurrences were uniformly driven by the sheer dominance of structurally static, high-thermal-inertia landscapes that lacked evaporative cooling during the pre-monsoon season. Because the analytical methodology required a region to consistently exceed a high-temperature threshold to be classified as a PTH, these intense thermal signatures only formed over landscapes devoid of rapid land-cover changes. Whether it was the degraded hillslopes and shifting agricultural tracts of the EH districts, or the topographically enclosed, barren terrains and flood plains of Balangir and Nayagarh, these environments all suffered from a profound absence of substantial vegetative canopy and soil moisture. Consequently, without plants or surface water to facilitate evaporative cooling, these bare, exposed surfaces absorbed maximum solar radiation and sustained extreme temperatures to be classified as PTHs consistently throughout the study period.

It would be prudent to note that since these hotspots represented chronic, structurally unchanging heat reservoirs, they could easily subject local communities to prolonged heat stress. To mitigate the PTH occurrences across these districts, a multi-pronged approach focusing on urban cooling and ecological restoration may be essential. In industrial and urban hubs like Sundergarh, Khordha, Jajpur, and Jagatsinghpur districts, mitigation should prioritize cool infrastructure by implementing reflective roofing, permeable pavements, and vertical gardens to counteract the high thermal inertia of concrete.[74] Expanding urban forestry and creating green corridors would provide critical shading and evaporative cooling, effectively mimicking a naturally vegetated region. For coastal districts like Baleswar, Bhadrak, and Kendrapara, protecting and expanding coastal mangrove ecosystems would prove to be vital. These dense mangrove canopies would offer superior thermal regulation and moisture retention compared to exposed sandy coastlines.[75] In the vast agricultural and riverine belts of Cuttack, Puri, Ganjam, and Nayagarh, the focus should shift toward sustainable land management and water conservation. For hotspots tracing the dry beds of the Mahanadi, Brahmani, and Baitarani rivers, integrated watershed management and the restoration of riparian vegetation would significantly enhance localized cooling. Furthermore, protecting the forested highlands of the Eastern Ghats would be equally crucial, as these natural thermal buffers would provide the regional moisture and shade necessary to stabilize temperatures in the adjacent heating plains.

3.4 Population exposure to thermal hotspots

While the identification of PTHs delineated the spatial distribution of long-term environmental heat, analyzing population exposure provided a crucial anthropogenic dimension to understanding this vulnerability. Analysis revealed clear inter-annual variability and regional heterogeneity in how this thermal stress impacted local communities. In terms of absolute numbers, districts like Ganjam, Sundargarh, Khordha, and Cuttack experienced the highest population exposure statewide. This vulnerability was primarily because these districts encompassed Odisha's major urban, commercial, and industrial centers. The high exposure in CP districts, like Khordha, Cuttack, and Ganjam, was driven by their status as dense metropolitan hubs characterized by extensive built environments and high population densities. Similarly, the elevated exposure in Sundargarh, situated in the NP region, was heavily influenced by anthropogenic heat generation stemming from large-scale industrial activities. Fig. 9 depicts the percentage of the total district population exposed to these hotspots. This approach provided a normalized intercomparable indicator of population exposure in the 30 districts of Odisha. The highest proportional exposures were consistently observed in the EH and select districts of the CP regions. Notably, Rayagada and Nayagarh demonstrated persistent vulnerability, recording significant exposure levels almost every year throughout the study period. Conversely, sub-regions within the NP and the majority of the CB districts displayed generally lower and less consistent exposure percentages. This trend suggested that these areas either possessed localized microclimates less susceptible to forming widespread thermal hotspots, or their populations were geographically distributed outside the primary heat zones. A closer temporal analysis of the seven-year period revealed distinct climatological and anthropogenic patterns. The years 2017 (Fig. 9a) and 2022 (Fig. 9f) stood out in the data, exhibiting high and widespread percentage exposure across multiple sub-regions, indicating periods of elevated, state-wide thermal stress. In contrast, the year 2020 (Fig. 9d) exhibited the lowest exposure to thermal hotspots across the entire dataset, with the metrics for almost all districts dropping notably. This reduction in exposed populations could directly be attributed to the pandemic-induced lockdowns, reducing major anthropogenic disruptions (industrial operations, vehicular traffic, and overall urban activity), leading to lower surface temperatures.[76]

Overall, the study's findings revealed that the proliferation of thermal hotspots in the built-up areas of Odisha's urbanizing

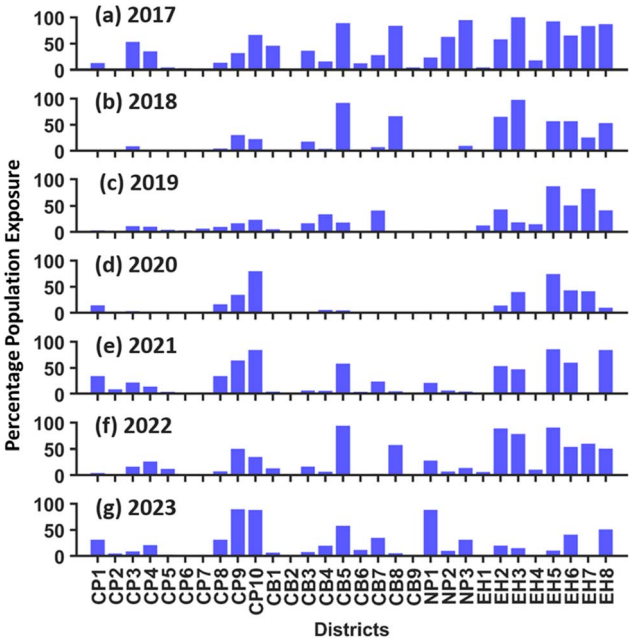

Fig. 9 Yearly percentage population exposure in the 30 districts of Odisha from 2017 to 2023.

districts, such as Khordha and Ganjam, was attributable to the transformation of natural, permeable surfaces into impervious ones like asphalt and concrete. These artificial materials possess higher thermal capacity, causing them to absorb more solar radiation and retain heat for longer periods. The observed increasing trend of hotspots in these specific districts directly reflected their ongoing, rapid infrastructure development and population growth. A particularly crucial finding was the geographical diversity in hotspot distribution, where the hotspots of western and interior districts like Bargarh and Kalahandi were governed by the thermal conditions in non-built-up areas. This challenged the simplistic view that only urban areas were prone to extreme heat. The prevalence of hotspots in these agrarian and semi-arid regions was driven by land degradation factors such as deforestation, barren lands, and fallow agricultural fields during the dry pre-monsoon season. This indicates that land management practices, not just urbanization, are critical drivers of regional thermal stress. The unique case of Sundargarh, which exhibited significant hotspots in both built-up and non-built-up areas, exemplified a complex scenario where industrial heating compounds the effects of degraded natural landscapes. Several studies have linked an increase in vector-borne diseases and human health issues with increasing temperatures and other climate extremes in Odisha.[18,20–22,37] The projected increase in population density in the urban-industrial regions will also enhance the exposure of its inhabitants to extreme heat. In such a situation, an increase in the frequency and coverage of urban thermal hotspots at the current rate would exacerbate this situation and pose a severe risk to sustainable and comfortable living, especially in the rapidly urbanizing regions of developing countries like India.[77] However, the significant drop in population exposure observed during the 2020 period suggests a viable countermeasure, demonstrating that implementing strategic, temporary reductions in urban and industrial activities, during peak thermal events could possibly serve as an effective, immediate policy tool to mitigate impacts of heat stress on vulnerable populations.

4. Conclusion

This study provides a comprehensive analysis of thermal hotspots across 30 districts of Odisha, India, focusing on the differences between built-up and non-built-up land covers during pre-monsoon seasons of 2017 to 2023. The findings revealed a significant increase in thermal hotspots in highly urbanized districts such as Khordha, Ganjam, Sundargarh, and Sambalpur, where rapid urban expansion and impervious surface growth contributed to increasing temperatures. Conversely, interior districts like Bargarh, Balangir, and Kalahandi exhibited more pronounced hotspot areas in non-built-up regions, primarily due to the conversion of natural vegetated land covers into fallow agricultural and barren lands. It was also observed that the abundance of paved surfaces and densely packed infrastructure led to an increase in persistent hotspots, whereas urban forests and vegetated regions helped alleviate the heat stress. Consequently, significant population exposure to thermal stress could be avoided with timely knowledge of PTHs. This study hence proposes targeted mitigation efforts in regions under extreme heat stress and thermal hotspot occurrences. Increasing urban greenery, implementing heat-resilient infrastructure, and promoting sustainable land-use policies that balance development with environmental conservation can help reduce surface heating, minimize health risks, and lead society towards a more harmonious living with nature.

Author contributions

DM – conceptualization, data curation, formal analysis, investigation, methodology, software, validation, visualization, writing – original draft; DS – conceptualization, investigation, methodology, resources, supervision, writing – original draft.

Conflicts of interest

The authors declare that they do not have any known competing interests whatsoever associated with this study.

Data availability

The present analysis was carried out by utilising various data sets available in the respective public domains. Sentinel-2 surface reflectances are available through the Copernicus Browser (https://browser.dataspace.copernicus.eu/), while Sentinel-2 LULC data sets can be obtained from the ArcGIS Living Atlas of the World (https://livingatlas.arcgis.com/en/home/). MODIS surface reflectances (MOD09A1.061, MYD09A1.061) and LST (MYD11A2.061) products are available at the NASA LP DAAC (https://www.earthdata.nasa.gov/data) and the yearly population counts at WorldPop Hub (https://hub.worldpop.org/geodata/listing?id=135).

Acknowledgements

The authors acknowledge IIT Bhubaneswar for providing the infrastructure to carry out this study and the various agencies for providing the satellite data used in this work. The authors are also grateful to the anonymous reviewers whose comments and suggestions have contributed to improving the manuscript contents immensely.

References

1 E. F. Lambin, H. J. Geist and E. Lepers, Dynamics of land-use and land-cover change in tropical regions, *Annu. Rev. Environ. Resour.*, 2003, **28**(1), 205–241, DOI: 10.1146/annurev.energy.28.050302.105459.

2 D. Swain, G. J. Roberts, J. Dash, K. Lekshmi, V. Vinoj and S. Tripathy, Impact of rapid urbanization on the city of Bhubaneswar, India, *Proc. Nat. Acad. Sci. India Sect. A*, 2017, **87**(4), 845–853, DOI: 10.1007/s40010-017-0453-7.

3 P. S. Roy, R. M. Ramachandran, O. Paul, P. K. Thakur, S. Ravan, M. D. Behera, *et al.*, Anthropogenic land use and land cover changes—A review on its environmental consequences and climate change, *J. Ind. Soc. Remote Sens.*, 2022, **50**(8), 1615–1640, DOI: 10.1007/s12524-022-01569-w.

4 M. Santamouris, Regulating the damaged thermostat of the cities—Status, impacts and mitigation challenges, *Energy Build*, 2015, **91**, 43–56, DOI: 10.1016/j.enbuild.2015.01.027.

5 J. S. Golden, The built environment induced urban heat island effect in rapidly urbanizing arid regions-a sustainable urban engineering complexity, *Environ. Sci.*, 2004, **1**(4), 321–349.

6 M. O. Obiakor, C. D. Ezeonyejiaku and T. C. Mogbo, Effects of vegetated and synthetic (impervious) surfaces on the microclimate of urban area, *J. Appl. Sci. Environ. Manag.*, 2012, **16**(1), 85–94.

7 P. Devanathan, K. Devanathan. Heat island effects. in *Green Building with Concrete: Sustainable Design Construction*, ed. G. M. Sabnis, Taylor & Francis, London, England, 2011. pp. 175–226. https://bayanbox.ir/view/3322753378973510188/1439812969-a.pdf.

8 A. K. Hua and O. W. Ping, The influence of land-use/land-cover changes on land surface temperature: a case study of Kuala Lumpur metropolitan city, *Eur. J. Remote Sens.*, 2018, **51**(1), 1049–1069, DOI: 10.1080/22797254.2018.1542976.

9 A.-A. Kafy, M. S. Rahman, A.-A. Faisal, M. M. Hasan and M. Islam, Modelling future land use land cover changes and their impacts on land surface temperatures in Rajshahi, Bangladesh, *Remote Sens. Appl. Soc. Environ.*, 2020, **18**(100314), 100314, DOI: 10.1016/j.rsase.2020.100314.

10 M. Ramzan, Z. A. Saqib, E. Hussain, J. A. Khan, A. Nazir, M. Y. S. Dasti, *et al.*, Remote sensing-based prediction of temporal changes in land surface temperature and land use-land cover (LULC) in urban environments, *Land*, 2022, **11**(9), 1610, DOI: 10.3390/land11091610.

11 R. Yao, L. Wang, X. Huang, W. Gong and X. Xia, Greening in rural areas increases the surface urban heat island intensity, *Geophys. Res. Lett.*, 2019, **46**(4), 2204–2212, DOI: 10.1029/2018gl081816.

12 K. J. Gohain, P. Mohammad and A. Goswami, Assessing the impact of land use land cover changes on land surface temperature over Pune city, India, *Quat. Int.*, 2021, **575–576**, 259–269, DOI: 10.1016/j.quaint.2020.04.052.

13 K. Srikanth and D. Swain, Urbanization and Land surface temperature changes over Hyderabad, a semi-arid mega city in India, *Remote Sens. Appl. Soc. Environ.*, 2022, **28**(100858), 100858, DOI: 10.1016/j.rsase.2022.100858.

14 Q. Weng, Thermal infrared remote sensing for urban climate and environmental studies: Methods, applications, and trends, *ISPRS J. Photogramm. Remote Sens.*, 2009, **64**(4), 335–344, DOI: 10.1016/j.isprsjprs.2009.03.007.

15 Y. Kestens, A. Brand, M. Fournier, S. Goudreau, T. Kosatsky, M. Maloley, *et al.*, Modelling the variation of land surface temperature as determinant of risk of heat-related health events, *Int. J. Health Geogr.*, 2011, **10**(1), 7. https://www.ij-healthgeographics.com/content/10/1/7.

16 J. L. White-Newsome, S. J. Brines, D. G. Brown, J. T. Dvonch, C. J. Gronlund, K. Zhang, *et al.*, Validating satellite-derived land surface temperature with in situ measurements: a public health perspective, *Environ. Health Perspect.*, 2013, **121**(8), 925–931, DOI: 10.1289/ehp.1206176.

17 A. M. Abdel-Ghany, I. M. Al-Helal and M. R. Shady, Human thermal comfort and heat stress in an outdoor urban arid environment: A case study, *Adv. Meteorol.*, 2013, **2013**, 1–7, DOI: 10.1155/2013/693541.

18 A. Mohammadi, B. Mashhoodi, A. Shamsoddini, E. Pishgar and R. Bergquist, Land surface temperature predicts mortality due to chronic obstructive pulmonary disease: a study based on climate variables and impact machine learning, *Geospat. Health*, 2025, **20**(1), 40143752, DOI: 10.4081/gh.2025.1319.

19 P. Wang, Y. Yang, H. Li, L. Chen, R. Dang, D. Xue, *et al.*, North China Plain as a hot spot of ozone pollution exacerbated by extreme high temperatures, *Atmos. Chem. Phys.*, 2022, **22**(7), 4705–4719, DOI: 10.5194/acp-22-4705-2022.

20 G. Savioli, C. Zanza, Y. Longhitano, A. Nardone, A. Varesi, I. F. Ceresa, *et al.*, Heat-related illness in emergency and critical care: Recommendations for recognition and management with medico-legal considerations, *Biomedicines*, 2022, **10**(10), 2542, DOI: 10.3390/biomedicines10102542.

21 F. G. O'Connor, Heat-related illnesses, *Ann. Intern. Med.*, 2025, **178**(7), ITC97–112, DOI: 10.7326/ANNALS-25-01958.

22 G. P. Kenny, J. Yardley, C. Brown, R. J. Sigal and O. Jay, Heat stress in older individuals and patients with common chronic diseases, *Canadian Med. Assoc. J.*, 2010, **182**(10), 1053–1060, DOI: 10.1503/cmaj.081050.

23 R. C. Estoque, Y. Murayama and S. W. Myint, Effects of landscape composition and pattern on land surface temperature: An urban heat island study in the megacities of Southeast Asia, *Sci. Total Environ.*, 2017, **577**, 349–359, DOI: 10.1016/j.scitotenv.2016.10.195.

24 A. Caseiro, G. Rücker, J. Tiemann, D. Leimbach, E. Lorenz, O. Frauenberger, *et al.*, Persistent Hot Spot detection and characterisation using SLSTR, *Remote Sens.*, 2018, **10**(7), 1118, DOI: 10.3390/rs10071118.

25 T. Mavrakou, A. Polydoros, C. Cartalis and M. Santamouris, Recognition of thermal hot and cold spots in urban areas in support of mitigation plans to counteract overheating: Application for Athens, *Climate*, 2018, **6**(1), 16, DOI: 10.3390/cli6010016.

26 P. Zhang, C. Yuan, Q. Sun, A. Liu, S. You, X. Li, *et al.*, Satellite-based detection and characterization of industrial heat sources in China, *Environ. Sci. Technol.*, 2019, **53**(18), 11031–11042, DOI: 10.1021/acs.est.9b02643.

27 D. Mullerova and M. Williams, Satellite monitoring of thermal performance in smart urban designs, *Remote Sens.*, 2019, **11**(19), 2244, DOI: 10.3390/rs11192244.

28 Z. Wang, X. Sun and H. Wang, Threshold-driven modeling of urban heat exposure under impervious surface expansion: a decadal remote sensing assessment of Shanghai, *Stoch. Environ. Res. Risk Assess.*, 2026, **40**(1), 5, DOI: 10.1007/s00477-025-03150-6.

29 P. Karami and S.-M. Mousavi, Spatiotemporal analysis of thermal islands in a semi-arid city: A case study of Kermanshah, Iran using machine learning and remote sensing, *Environ. Challang.*, 2025, **20**(101174), 101174, DOI: 10.1016/j.envc.2025.101174.

30 J. Sola-Caraballo, A. Serrano-Jiménez, C. Rivera-Gomez and C. Galan-Marin, Multi-criteria assessment of urban thermal hotspots: A GIS-based remote sensing approach in a Mediterranean climate city, *Remote Sens.*, 2025, **17**(2), 231, DOI: 10.3390/rs17020231.

31 S. Kumari, R. Singh, V. B. Singh and V. Chauhan, A multivariate geostatistical framework to assess the spatio-temporal dynamics of coupled urban–thermal–ecological interactions in the western Himalaya foothills, *Geosystems Geoenviron.*, 2026, **5**(2), 100497, DOI: 10.1016/j.geogeo.2026.100497.

32 R. Maroofiazar and A. M. Reveshti, Integrating Remote Sensing and Machine Learning for Enhanced Surface Urban Heat Island Analysis and Its Impact on Building Energy Demand, *Energy Sci. Eng.*, 2026, **14**(4), 2051–2069, DOI: 10.1002/ese3.70463.

33 N. Eingrüber, N. Burdová, V. Dlugoß, A. Domm, M. Bongartz and U. Nehren, Hotspots in urban areas: A novel approach to assess the heat mitigation potential of nature-based solutions using microclimate modelling, *Urban Clim.*, 2026, **65**(102814), 102814, DOI: 10.1016/j.uclim.2026.102814.

34 D. M. Moges, K. Mattisson, E. Malmqvist and P.-O. Olsson, Remote sensing of urban heat dynamics and the cooling effect of urban green spaces in Ethiopian cities, *Environ Challang.*, 2026, **23**(101462), 101462, DOI: 10.1016/j.envc.2026.101462.

35 Z.-L. Li, B.-H. Tang, H. Wu, H. Ren, G. Yan, Z. Wan, *et al.*, Satellite-derived land surface temperature: Current status and perspectives, *Remote Sens. Environ.*, 2013, **131**, 14–37, DOI: 10.1016/j.rse.2012.12.008.

36 I. Agathangelidis and C. Cartalis, Improving the disaggregation of MODIS land surface temperatures in an urban environment: a statistical downscaling approach using high-resolution emissivity, *Int. J. Remote Sens.*, 2019, **40**(13), 5261–5286, DOI: 10.1080/01431161.2019.1579386.

37 Q. Mao, J. Peng and Y. Wang, Resolution enhancement of remotely sensed land surface temperature: Current status and perspectives, *Remote Sens.*, 2021, **13**(7), 1306, DOI: 10.3390/rs13071306.

38 S. Mukherjee, P. K. Joshi and R. D. Garg, Evaluation of LST downscaling algorithms on seasonal thermal data in humid subtropical regions of India, *Int. J. Remote Sens.*, 2015, **36**(10), 2503–2523, DOI: 10.1080/01431161.2015.1041175.

39 X. Feng, G. Foody, P. Aplin and S. N. Gosling, Enhancing the spatial resolution of satellite-derived land surface temperature mapping for urban areas, *Sustain. Cities Soc.*, 2015, **19**, 341–348, DOI: 10.1016/j.scs.2015.04.007.

40 N. Agam, W. P. Kustas, M. C. Anderson, F. Li and C. M. U. Neale, A vegetation index based technique for spatial sharpening of thermal imagery, *Remote Sens. Environ.*, 2007, **107**(4), 545–558, DOI: 10.1016/j.rse.2006.10.006.

41 X.-L. Chen, H.-M. Zhao, P.-X. Li and Z.-Y. Yin, Remote sensing image-based analysis of the relationship between urban heat island and land use/cover changes, *Remote Sens. Environ.*, 2006, **104**(2), 133–146, DOI: 10.1016/j.rse.2005.11.016.

42 S. Guha and H. Govil, A long-term monthly analytical study on the relationship of LST with normalized difference spectral indices, *Eur. J. Remote Sens.*, 2021, **54**(1), 487–512, DOI: 10.1080/22797254.2021.1965496.

43 B. Banerjee, A. Pal, A. K. Tiwari and R. Kanchan, Assessing the land use dynamics and thermal environment using geospatial techniques in the industrial city of Chotanagpur Plateau Region, India, *Environ. Monit. Assess.*, 2024, **196**(7), 609, DOI: 10.1007/s10661-024-12752-6.

44 M. Karmakar and M. M. Pradhan, Climate change and public health: a study of vector-borne diseases in Odisha, India, *Nat. Hazards*, 2020, **102**(2), 659–671, DOI: 10.1007/s11069-019-03594-4.

45 India Meteorological Department, *Climate of Orissa*, 2002, https://imdpune.gov.in/library/public/climate20of20orissa.pdf.

46 Government of India, *A-01: Number of Villages, Towns, Households, Population and Area (India, states/UTs, Districts and Sub-districts)*, Census India, 2011, https://censusindia.gov.in/census.website/data/census-tables.

47 T. G. Farr, P. A. Rosen, E. Caro, R. Crippen, R. Duren, S. Hensley, *et al.*, The Shuttle Radar Topography Mission, *Rev. Geophys.*, 2007, **45**(2), RG2004, DOI: 10.1029/2005rg000183.

48 S. Safieddine, C. Clerbaux, J. Muñoz-Sabater and J.-N. Thépaut, Local hourly trends in near-surface and land surface temperatures, *Sci. Rep.*, 2025, **15**(1), 29915, DOI: 10.1038/s41598-025-15731-0.

49 P. Hesslerová, J. Pokorný, J. Brom and A. Rejšková - Procházková, Daily dynamics of radiation surface temperature of different land cover types in a temperate cultural landscape: Consequences for the local climate, *Ecol. Eng.*, 2013, **54**, 145–154, DOI: 10.1016/j.ecoleng.2013.01.036.

50 J. W. Rouse, R. H. Haas, J. A. Schell, D. W. Deering and J. C. Harlan. Monitoring the vernal advancement and retrogradation (greenwave effect) of natural vegetation. *NASA/GSFC Type III Final Report*. 1974.

51 Y. Zha, S. Y. Ni and S. Yang, An Effective Approach to Automatically Extract Urban Land-Use from TM Imagery, *J. Remote Sens*, 2003, **7**(1), 37–40.

52 H. Zhao and X. Chen. Use of normalized difference bareness index in quickly mapping bare areas from TM/ETM+. in *Proceedings 2005 IEEE International Geoscience and Remote Sensing Symposium, 2005 IGARSS '05*. IEEE, 2005.

53 S. Jin and S. A. Sader, Comparison of time series tasseled cap wetness and the normalized difference moisture index in detecting forest disturbances, *Remote Sens. Environ.*, 2005, **94**(3), 364–372, DOI: 10.1016/j.rse.2004.10.012.

54 M. Feng, C. Huang, S. Channan, E. F. Vermote, J. G. Masek and J. R. Townshend, Quality assessment of Landsat surface reflectance products using MODIS data, *Comput. Geosci.*, 2012, **38**(1), 9–22, DOI: 10.1016/j.cageo.2011.04.011.

55 S. Liang, H. Fang, M. Chen, C. J. Shuey, C. Walthall, C. Daughtry, *et al.*, Validating MODIS land surface reflectance and albedo products: methods and preliminary results, *Remote Sens. Environ.*, 2002, **83**(1–2), 149–162, DOI: 10.1016/s0034-4257(02)00092-5.

56 S. Misbari, W. Zhai and S. I. Doh, Comparative analysis between Landsat and MODIS data for urban heat island mapping in Kuala Lumpur, *Constr*, 2025, **5**(2), 139–145, DOI: 10.15282/construction.v5i2.12436.

57 S. Zhu, H. Zhang, R. Liu, Y. Cao and G. Zhang, Comparison of sampling designs for estimating deforestation from landsat TM and MODIS imagery: a case study in Mato Grosso, *Sci. World J.*, 2014, **2014**, 919456, DOI: 10.1155/2014/919456.

58 T. Lv, X. Zhou, Z. Tao, X. Sun, J. Wang, R. Li, *et al.*, Remote sensing-guided spatial sampling strategy over heterogeneous surface ground for validation of vegetation indices products with medium and high spatial resolution, *Remote Sens.*, 2021, **13**(14), 2674, DOI: 10.3390/rs13142674.

59 T. Zhao, X. Zhang, Y. Gao, J. Mi, W. Liu, J. Wang, *et al.*, Assessing the accuracy and consistency of six fine-resolution global Land Cover products using a novel stratified random sampling validation dataset, *Remote Sens.*, 2023, **15**(9), 2285, DOI: 10.3390/rs15092285.

60 E. Massaro, R. Schifanella, M. Piccardo, L. Caporaso, H. Taubenböck, A. Cescatti, *et al.*, Spatially-optimized urban greening for reduction of population exposure to land surface temperature extremes, *Nat. Commun.*, 2023, **14**(1), 2903, DOI: 10.1038/s41467-023-38596-1.

61 M. F. Goodchild, L. Anselin and U. Deichmann, A framework for the areal interpolation of socioeconomic data, *Environ. Plan A*, 1993, **25**(3), 383–397, DOI: 10.1068/a250383.

62 Z. Wu and Y. Zhang, Water bodies' cooling effects on urban land daytime surface temperature: Ecosystem service reducing heat island effect, *Sustainability*, 2019, **11**(3), 787, DOI: 10.3390/su11030787.

63 Y. Jiang, J. Huang, T. Shi and H. Wang, Interaction of urban rivers and green space morphology to mitigate the urban heat island effect: Case-based comparative analysis, *Int. J. Environ. Res. Public Health*, 2021, **18**(21), 11404, DOI: 10.3390/ijerph182111404.

64 L. Chen, Q. Qi, H. Wu, D. Feng and E. Zhu, Will the landscape composition and socio-economic development of coastal cities have an impact on the marine cooling effect?, *Sustain. Cities Soc.*, 2023, **89**(104328), 104328, DOI: 10.1016/j.scs.2022.104328.

65 M. Tarawally, W. Xu, W. Hou and T. Mushore, Comparative analysis of responses of land surface temperature to long-term land use/cover changes between a coastal and inland city: A case of Freetown and Bo town in Sierra Leone, *Remote Sens.*, 2018, **10**(1), 112, DOI: 10.3390/rs10010112.

66 G. Jeon, Y. Park and J.-M. Guldmann, Impacts of urban morphology on seasonal land surface temperatures: Comparing grid- and block-based approaches, *ISPRS Int. J. Geoinf.*, 2023, **12**(12), 482, DOI: 10.3390/ijgi12120482.

67 R. R. Andriambololonaharisoamalala, P. Helmholz, D. Bulatov, I. Ivanova, Y. Song, S. Soon, *et al.*, Downscaling of urban land surface temperatures using geospatial machine learning with Landsat 8/9 and Sentinel-2 imagery, *Remote Sens.*, 2025, **17**(14), 2392, DOI: 10.3390/rs17142392.

68 A. Ibe A and M. Ogbodo C, Correlation analysis of compaction properties of soil with various soil parameters over Gbaramatu Niger Delta, Nigeria, *Earth Sci.*, 2023, **7**(2), 96–102, DOI: 10.26480/esmy.02.2023.96.102.

69 Census of India, *Primary Census Abstract - Data Highlights for Odisha (Series 22)*, 2011, [cited 2026 Mar 21]. https://censusindia.gov.in/nada/index.php/catalog/11313/download/14425/PC11_PCA_Data_Highlights_Odisha.pdf.

70 F. Liu, X. Zhang, Y. Murayama and T. Morimoto, Impacts of land cover/use on the urban thermal environment: A comparative study of 10 megacities in China, *Remote Sens.*, 2020, **12**(2), 307, DOI: 10.3390/rs12020307.

71 G. Guerri, A. Crisci, A. Messeri, L. Congedo, M. Munafò and M. Morabito, Thermal summer diurnal Hot-Spot analysis: The role of local urban features layers, *Remote Sens.*, 2021, **13**(3), 538, DOI: 10.3390/rs13030538.

72 L. Bounoua, R. DeFries, G. J. Collatz, P. Sellers and H. Khan, Effects of land cover conversion on surface climate, *Clim. Change*, 2002, **52**(1–2), 29–64, DOI: 10.1023/a:1013051420309.

73 A. Halefom, Y. He, T. Nemoto, L. Feng, R. Li, V. Raghavan, *et al.*, The impact of urbanization-induced land use change on land surface temperature, *Remote Sens.*, 2024, **16**(23), 4502, DOI: 10.3390/rs16234502.

74 M. Santamouris, A. Synnefa and T. Karlessi, Using advanced cool materials in the urban built environment to mitigate heat islands and improve thermal comfort conditions, *Sol. Energy*, 2011, **85**(12), 3085–3102, DOI: 10.1016/j.solener.2010.12.023.

75 A. A. Al-huqail, Z. Islam and H. F. Al-Harbi, Mangroves trend and their impact on surface temperature in Al-Wajh Lagoon: a study aligned with Saudi Arabia's vision 2030, *Front. Environ. Sci.*, 2024, **12**, 1439425, DOI: 10.3389/fenvs.2024.1439425.
76 D. Nanda, D. R. Mishra and D. Swain, COVID-19 lockdowns induced land surface temperature variability in mega urban agglomerations in India, *Environ. Sci.:Processes Impacts*, 2021, **23**(1), 144–159, DOI: 10.1039/d0em00358a.
77 Intergovernmental Panel on Climate Change (IPCC), *Climate Change 2022 – Impacts, Adaptation and Vulnerability: Working Group II Contribution to the Sixth Assessment Report of the Intergovernmental Panel on Climate Change*, Cambridge University Press, Cambridge, England, 2023. DOI: 10.1017/9781009325844.